International Scholarly Research Network
ISRN Nanotechnology
Volume 2012, Article ID 532168, 8 pages
doi:10.5402/2012/532168

Research Article

Electrochemical Synthesis of Nanocrystalline $Ni_{0.5}Zn_{0.5}Fe_2O_4$ Thin Film from Aqueous Sulfate Bath

A. Saba,[1] E. Elsayed,[1] M. Moharam,[1] and M. M. Rashad[2]

[1] *Mineral Processing Technology Department, Central Metallurgical Research and Development Institute (CMRDI), P.O. Box 87, Helwan, Cairo 11421, Egypt*
[2] *Advanced Materials Department, Central Metallurgical Research and Development Institute (CMRDI), P.O. Box 87, Helwan, Cairo 11421, Egypt*

Correspondence should be addressed to M. M. Rashad, rashad133@yahoo.com

Received 29 December 2011; Accepted 22 February 2012

Academic Editors: J. Blázquez, J.-H. Chang, G. Maruccio, and C.-S. Yeh

Nanocrystalline nickel-zinc ferrites $Ni_{0.5}Zn_{0.5}Fe_2O_4$ thin films have been synthesized via the electrodeposition-anodization from the aqueous sulfate bath. The electrodeposited (Ni-Zn)Fe_2 alloy was anodized in aqueous 1 M KOH solution to form the corresponding hydroxides which annealed at different temperatures ranging from 800 to 1000°C for various periods from 1 to 4 h, to get the required ferrite. SEM micrograph of the formed ferrite particles, annealed at 1000°C for 4 h appeared as the octahedral-like structure. A good saturation magnetization of 28.2 emu/g was achieved for $Ni_{0.5}Zn_{0.5}Fe_2O_4$ thin film produced after the aforementioned conditions. The kinetic studies of the crystallization of $Ni_{0.5}Zn_{0.5}Fe_2O_4$ films appeared to be first-order reaction and the activation energy was found to be 10.5 k Joule/mole.

1. Introduction

In recent years, soft magnetic Ni-Zn ferrite films with good magnetic properties, high resistivity, and low coercivity have critical need for high-frequency applications such as RF broad "band choke band," planar inductors, magnetic sensors, transformers cores, rod antennas, microwaves devices, and telecommunication [1–6]. Therefore, numerous deposition techniques are used for synthesis of required ferrites thin films. They include ferrite plating [7], chemical vapor deposition [8], sputtering [7], dip coating [9], spray pyrolysis [10], and pulsed laser deposition [11] processes. The main difficulties of these methods are that the substrate during or after deposition must be kept at high temperatures, which imposes restrictions on the selection of the substrate material [7]. Also, some of these processes require expensive equipment for a high degree of control. Furthermore, on sintering, the possibility of nonreproducible products and toxic gases are produced [12]. To avoid the problems arising from the high-temperature processes, room temperature synthesis of metal ferrites thin films using electrochemical deposition methods has attracted much attention [13, 14]. In comparison, the electrodeposition technique provides not only the possibility of using low synthesis temperature but also low cost of starting materials and a high purity of the product yield [15–17].

In our previous work, Ni-Zn ferrites thin films have been synthesized via the electrodeposition from ethylene glycol nonaqueous solution [13]. The results obtained indicate the production of $Ni_xZn_{1-x}Fe_2O_4$. A high saturation magnetization (48 emu/g) is achieved for $Ni_{0.5}Zn_{0.5}Fe_2O_4$ phase. The activation energy of its crystallization is found to be 32 kJ/mol.

The present study aims to prepare $Ni_{0.5}Zn_{0.5}Fe_2O_4$ thin film using the aqueous electrochemical deposition method. The electrochemical properties were examined using galvanostatic and cyclic voltammetry. The changes in the crystal structure, crystallite size, microstructure, and magnetic properties of the produced ferrite films were investigated by X-ray diffraction (XRD), scanning electron microscope (SEM),

and vibrating sample magnetometer (VSM) techniques. Moreover, the reaction kinetics and the activation energy were determined.

2. Experimental

The Electrodeposition of (Ni-Zn)Fe_2 alloys were conducted from aqueous bath containing 0.1 M $NiSO_4$, 0.1 M $ZnSO_4$ and 0.1 M $(NH_4)_2Fe(SO_4)_2$. All solutions were prepared, immediately before each experiment by dissolving the requisite amount of analytically grade metal sulfates in de-ionized water. The substrate used was copper as a cathode and pure graphite rod as anode. The bath was stirred at 800 rpm.

Cyclic voltammetric (CV) tests were performed at room temperature using a conventional three-electrode cell, in which copper was used as working electrode, the auxiliary electrode was a graphite rod. The reference electrode used was a saturated mercurous sulfate electrode (MSE), E = 650 mV versus standard hydrogen electrode (SHE). The deposition potentials were determined from the polarization curves. Cyclic voltammograms were performed with a computer-controlled potentiostat (Volta-lab 21).

Electrodeposition was identified galvanostatically using constant currents ranging from 0.25 to 1A. Apparent current densities were obtained by dividing the applied current by macroscopic surface area of the deposit. The deposition conditions were optimized to get good quality of (Ni-Zn) Fe_2 alloy films with maximum thickness.

The alloy films were anodized using aqueous 1 M KOH. The anodization current density and time were optimized to get well-adhered oxide films to the substrates. After anodization, the films were washed with distilled water and annealed after drying.

The crystalline phases in the different annealed ferrite samples were investigated using X-ray diffraction (XRD) on a Brucker axis D8 diffractometer using the Cu-Kα (λ = 1.5406 A°) radiation and secondary monochromator in the range 2θ from 20° to 80°. The ferrite particle morphologies were examined by Scanning Electron Microscope (SEM) (JEOL—model JSM-5400). The magnetic properties of the ferrites were measured at room temperature using a vibrating sample magnetometer VSM (9600-1 LDJ, USA) in a maximum applied field of 15 kOe. From the obtained hysteresis loops, the saturation magnetization M_s, remanence magnetization ratio M_r, and coercivity H_c were determined.

3. Results and Discussion

3.1. Cyclic Voltammetry (CV). Figures 1(a)–1(f) showed the cyclic voltammogram (CV) of 0.1 M of $ZnSO_4$, $NiSO_4$, $(NH_4)_2Fe(SO_4)_2$, Ni-Zn alloy, Ni-Fe alloy, and (Ni-Zn)Fe_2 alloy, respectively, from aqueous sulfate bath. Voltammetric studies were performed within the range of 0 to −2 V using a scan rate (S.R.) of 10 mV s^{-1}. Cyclic voltammogram of $ZnSO_4$ (Figure 1(a)) was characterized by one cathodic peak (C) and one anodic peak (A). This cathodic peak appeared at potential around (E = −0.97 V) for nonagitated solution and at −0.48 V when stirred at 1400 rpm (C_1). This cathodic peak represents the reduction of zinc (II) ions to metallic zinc (1). In previous studies, the reduction process associated with this peak is controlled by mass transfer mechanism [18]

$$Zn^{+2} + 2e^- \longleftrightarrow Zn \quad (1)$$

On reversing the scan in positive direction at −2 V an anodic peak appeared around −0.7 V for nonstirred solution and −0.5 V for agitated one. This peak is associated with the oxidation of metallic zinc, formed during the scan in negative direction. Moreover, the cathodic current densities were shifted from −5 mA cm^{-2} for nonagitated solution to, −12.8 mA cm^{-2} for agitated ones.

In comparison, the CV of 0.1 M of $NiSO_4$ (Figure 1(b)) is characterized by one cathodic peak at potential −0.59 V. For instance, increasing the agitation rate from 0 to 1400 rpm, the cathodic potential shifted from −0.59 to −0.50 V and the current density changed from −6.3 to −18.2 mA cm^{-2}. The increment in the current densities values can be ascribed to the hydrogen evolution reaction.

Figure 1(c) shows the CV of 0.1 M of ammonium ferrous sulfate solution. Iron electrodeposited is observed at potential −0.45 V, and on reversing the scan direction anodic peak appeared at potential −0.68 V for nonstirred solution. However, agitating the solution shifts the current density from −0.7 A cm^{-2} for nonstirred solution to −2.2 A cm^{-2} for the agitated solution at 1400 rpm.

Figure 1(d) represents the cyclic voltammogram of Ni-Zn alloy. It is clear that one cathodic peak (C) was formed at (E = −0.89 V) for nonagitated solution. This peak probably represents the codeposition of Ni-Zn alloy. However, this cathodic peak was shifted to −0.58 V on agitating the solution. For instance, agitating the solution increased the current density from −39 to −91 mA cm^{-2}. Two anodic peaks were appeared when the scan is performed in the positive direction, (A_1, A_2) at (E = −0.850, V = −0.185 V). The anodic peaks: A_1 represents the dissolution of zinc metal, while A_2 represents the dissolution of Ni-Zn alloy [19].

Cyclic voltammogram in Figure 1(e) is characterized by one cathodic peak (E = −0.80 V) which is supposed to be for the electrodeposition of Fe-Ni alloy with nonstirred solution and one anodic peak at −0.64 V which is supposed to be for the electrodissolution of Fe-Ni alloy. Increasing the agitation rate from 0 to 800 rpm shifted the current density from −0.77 to −1.27 A cm^{-2} while the codeposition potential was shifted from −0.80 to −0.53 V. Ni-Zn alloy and Fe-Ni alloy are considered as anomalous alloys [20].

Figure 1(f) represents the cyclic voltammograms for the electrodeposited (Ni-Zn)Fe_2 alloy. It is observed that one cathodic peak C (E = −0.58 V) was obtained with nonagitated solution. Agitating the solution shifted the cathodic potential peak to more positive one. For instance, the potential was shifted from −0.58 V for nonagitated solution to −0.57 V for agitated one at 1400 rpm. In addition, agitating the solution changed the solution cathodic current density from −52 to −172 mA cm^{-2}.

3.2. Chronoamperometric Study. Scharifker and Hills suggested model to describe the nucleation process during initial few seconds using chronoamperometric technique.

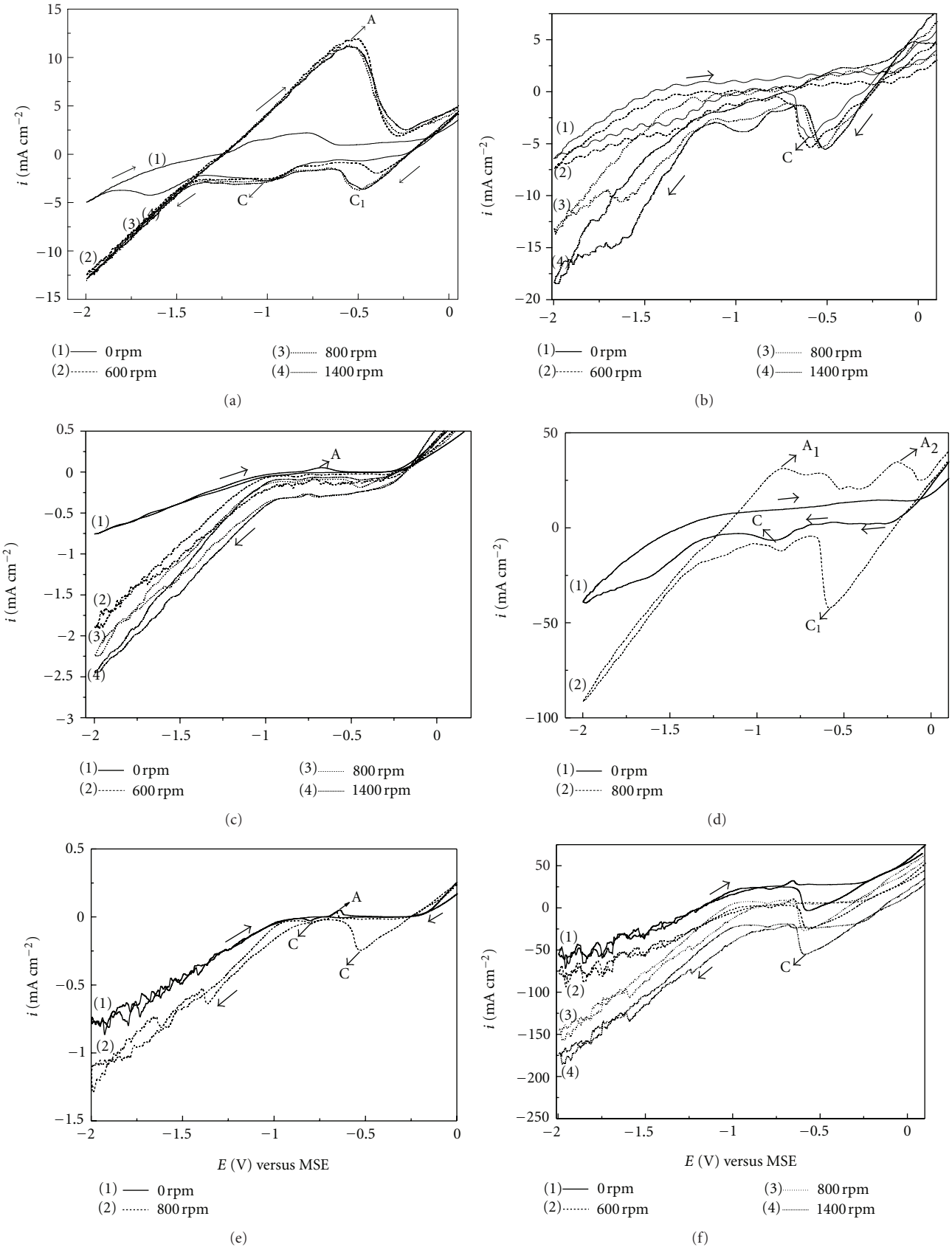

Figure 1: Voltammograms obtained on Cu electrode in aqueous solution of: (a) 0.1 M $ZnSO_4$, (b) $NiSO_4$, (c) $(NH_4)_2Fe(SO_4)_2$, (d) Ni-Zn alloy, (e) Ni-Fe alloy, and (f) $(Ni\text{-}Zn)Fe_2$ alloy.

The nucleation process may be either progressive or instantaneous. Progressive nucleation corresponds to slow growth of nuclei on a less number of active sites, all of these sites activated at the same time. Instantaneous nucleation corresponds to fast growth of nuclei on many active sites, all activated during the course of electroreduction [21].

Figure 2 represents the potentiostatic current versus time (I-t) transients for nucleation and growth of (Ni-Zn)Fe_2 alloy at different potentials ranging between 570 and 1400 mV. The transients were separated into three regions. The first region corresponds to short times ($t < 0.5$ s). In this region the decrease in the cathodic current density was related to the charging of a double layer. The second region is related to the crystal nucleation process and growth of the crystals formed during the first region. The cathodic current densities of this region achieve its maximum value. The third region corresponds to the decline in the current density, which represents the diffusion process [21].

The transients have been analyzed by comparing the chronoamperometric curves to the dimensionless theoretical curves for the diffusion-controlled nucleation and growth of crystals in three dimensions (3D) proposed by Saba et al. [13].

The expressions for the instantaneous and progressive nucleation are given by following equations, respectively [20],

$$\frac{i^2}{i_{\max}^2} = 1.9542\left[\frac{t_{\max}}{t}\right]\left\{1-\exp\left[-1.2564\frac{t}{t_{\max}}\right]\right\}^2, \quad (2)$$

$$\frac{i^2}{i_{\max}^2} = 1.2254\left[\frac{t_{\max}}{t}\right]\left\{1-\exp\left[-2.3367\left(\frac{t}{t_{\max}}\right)^2\right]\right\}^2, \quad (3)$$

where $i_{\max}$ and $t_{\max}$ are the maximum current density observed at the maximum time $t_{\max}$.

The fitting of the experimental curves for the theoretical curves was shown in Figures 3(a) and 3(b).

3.3. Preparation of the (Ni-Zn)Fe_2 Alloy. The current efficiency for electrodeposition of (Ni-Zn)Fe_2 alloy was studied at different current densities ranging from 52 to 204 mA cm^{-2} at 800 rpm stirring value for bath including zinc sulfate, nickel sulfate, and ammonium ferrous sulfate in Ni : Zn : Fe molar ratio 0.5 : 0.5 : 2 at room temperature.

According to Sartale et al. [22], the reduction of divalent cations, Ni (II), Zn (II), and Fe(II), is two-step process. the first step one electron takes up to make monovalent adsorbed cations Ni(I)ads, Fe(I)ads and Zn(I)ads and then the second electron takes it to deposited neutral atom. Hydrogen evolution due to reduction of protons was considered as side reaction [13]; side reaction reduced the current efficiency and the kinetics of the metals reduction. The current efficiency of the (Ni-Zn)Fe_2 alloy deposition was calculated using the simple relation:

$$\varphi = 100x\left(\frac{m_{\exp}}{m_{\text{th}}}\right), \quad (4)$$

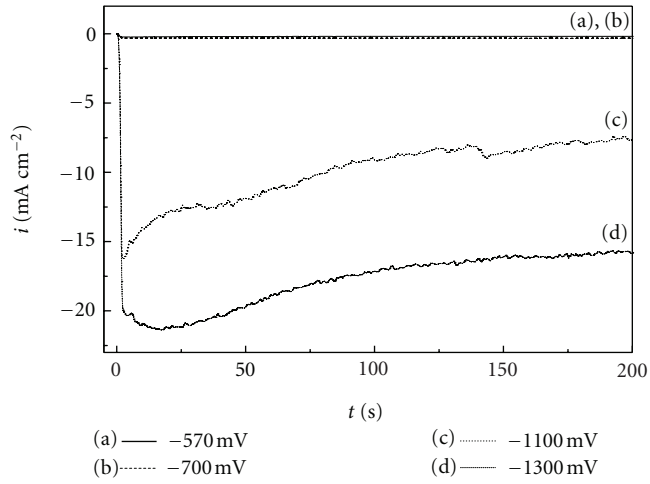

Figure 2: Chronoamperometric curves recorded at various electrode potentials ((a) −570 mV, (b) −700 mV, (c) −1100 mV, (d) −1300 mV) in aqueous solution of (Ni-Zn)Fe_2 alloy.

Table 1: The effect of current density on current efficiency for the electrodeposited (Ni-Zn) Fe_2 alloy.

Current density (mA/cm^2)	Current efficiency %
52	36.7
102	72.8
153	60.3
204	25.0

where $m_{\exp}$ and m_{th} are the experimental and theoretical masses of the (Ni-Zn)Fe_2 alloy. The theoretical mass of (Ni-Zn)Fe_2 alloy (m_{th}) can be calculated according to Faraday's law [23]. The change in the current efficiency with the current density is given in Table 1. The results showed that the current efficiency increases initially with increasing the current density up to 102 mA cm^{-2} and decreases afterwards within the range studied. About 72.8% current efficiency is obtained at current density of 102 mA cm^{-2}. With further increase in the current density up to 102 mA cm^{-2}, the protons reduction rate is higher than the deposition of metals (Figure 4). Further increase in the current density only leads to increase in the rate of hydrogen reduction which subsequently decreases the current efficiency [23].

3.4. Anodization of the Alloy. The anodization of (Ni-Zn)Fe_2 alloy thin film from the aqueous solution was performed using 1 M KOH at different annealing temperatures from 800 to 1000°C to form $Ni_{0.5}Zn_{0.5}Fe_2O_4$ films.

XRD diffraction patterns in Figure 5 show the produced $Ni_{0.5}Zn_{0.5}Fe_2O_4$ films at different annealing temperatures from 800 to 1000°C for 4 h. The results confirmed that the iron oxide α-Fe_2O_3 (JCPDS no. 73–603) is formed as impurity with the spinel $Ni_{0.5}Zn_{0.5}Fe_2O_4$ phase (JCPDS no.08–0234) at 800°C. Peaks at 2θ of 30.07, 35.42, 37.05, 43.09, 63.42, 56.94, 62.56, 71.02, 74.02 related to XRD diffraction planes (220), (311), (222), (400), (422), (511),

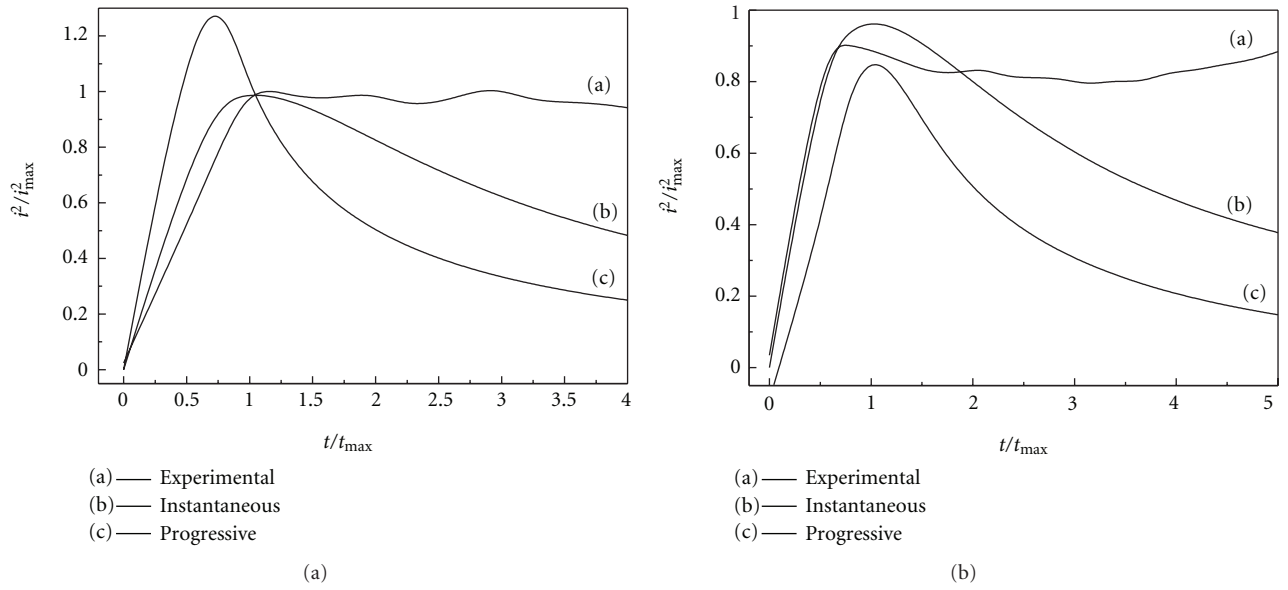

FIGURE 3: Nondimensional i^2/i^2_{max} versus t/t_{max} plots for electrodeposited (Ni-Zn)Fe_2 alloy at different potentials ((a) 570; (b) 1300 mV) for aqueous media.

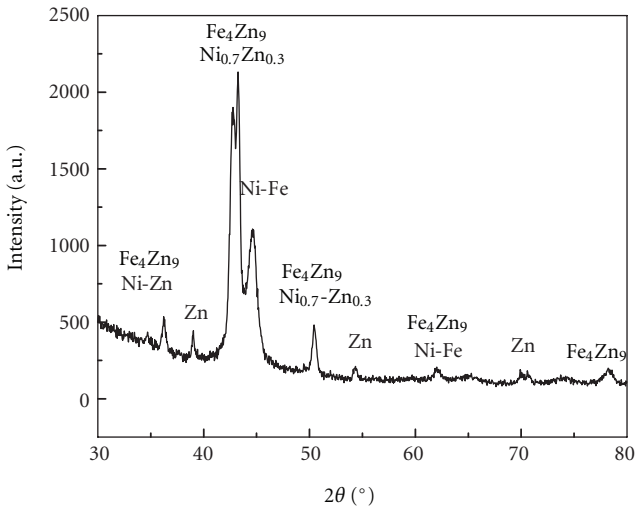

FIGURE 4: XRD patterns of (Ni-Zn)Fe_2 alloy electrodeposited from sulfate bath at current density 102 mA cm^{-2}.

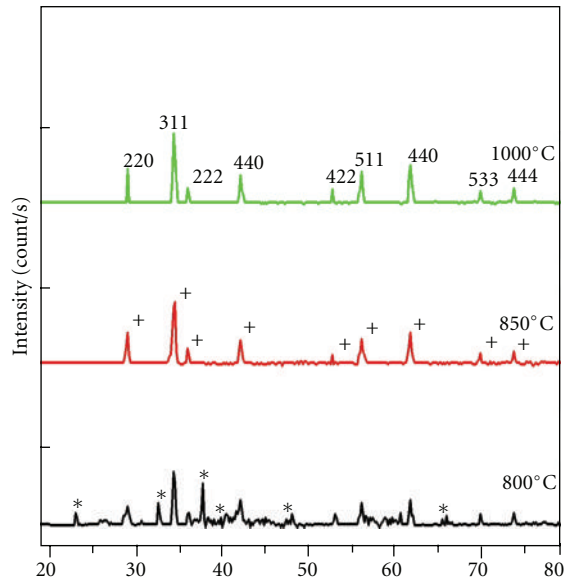

FIGURE 5: XRD patterns of the produced Ni-Zn ferrite at different annealing temperatures for 4 h.

(440), (620), and (533) of $Ni_{0.5}Zn_{0.5}Fe_2O_4$ phase are identified. Single phase of the spinel nickel zinc ferrite films appeared with increasing the annealing temperature from 850 to 1000°C. The crystallite sizes for the most intense peak (311) plane were estimated from XRD data based on Debye-Scherrer formula [13].The crystallite size of the ferrite films is increased with increasing the annealing temperature. Hence, it increased from 27 nm at 800 to 32 nm at 850°C then to 39 nm at 1000°C.

Figure 6 shows the SEM micrographs of $Ni_{0.5}Zn_{0.5}Fe_2O_4$ films annealed at (800, 850, 1000°C) for 4 h. The micrographs of $Ni_{0.5}Zn_{0.5}Fe_2O_4$ films in Figures 6(a) and 6(b) displayed spherical particles with a high agglomeration. Increasing annealing temperature to 1000°C octahedral-like structure was formed (Figure 6(c)).

Room-temperature M-H hysteresis loops of $Ni_{0.5}Zn_{0.5}Fe_2O_4$ thin film samples annealed at different temperatures are given in Figure 7. The results indicated that the saturation magnetization increased with increasing annealing temperature to 1000°C, as the result of the

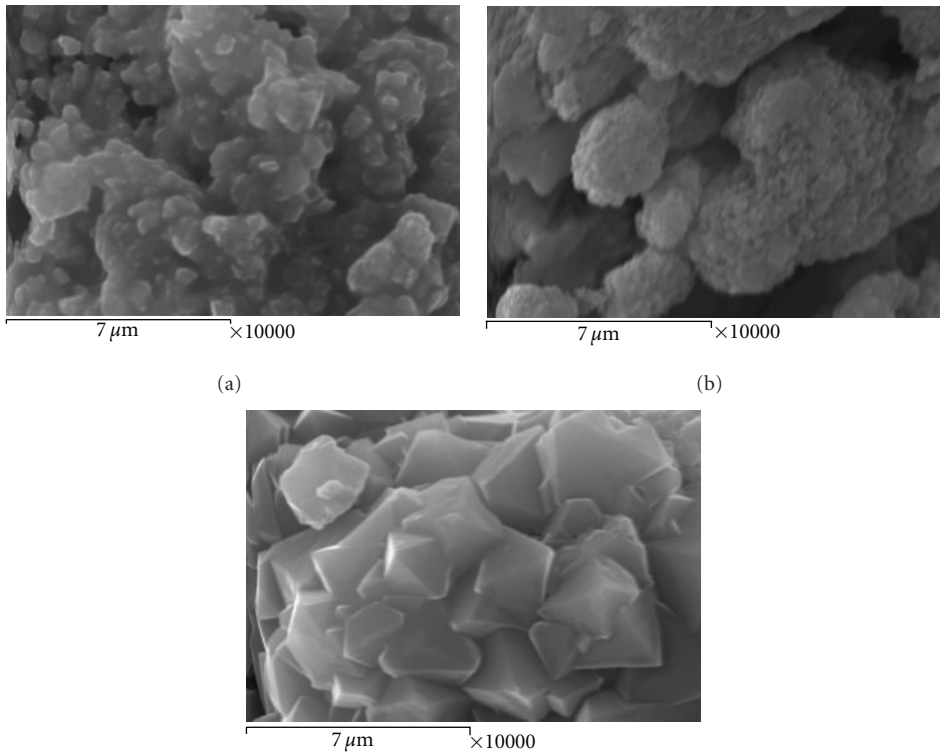

Figure 6: Effect of annealing temperature on the SEM patterns of $Ni_{0.5}Zn_{0.5}Fe_2O_4$ films. Annealing temperature: (a) 800°C, (b) 850°C, and (c) 1000°C.

increasing in the crystallite size, crystallinity, homogenous and clear microstructure. Furthermore, they indicated the decrease of the iron oxide content with increasing the annealing temperature. The H_c is intensively influenced from magnetic anisotropy including magnetocrystalline and strain-induced anisotropies. Increasing annealing temperature resulted in a decrease in crystal defects and internal strains. As a result, the coercivity was decreased due to a decrease in magnetic anisotropy and increasing the crystallite size [13, 24].

The value of saturation magnetization is lower than the previous obtained value by the authors for $Ni_{0.5}Zn_{0.5}Fe_2O_4$ powders (M_s = 85 emu/g) synthesized via the coprecipitation method [24]. Furthermore, the value is also lower than the value obtained of film using the electrodeposition from nonaqueous medium (M_s = 48.0 emu/g) using ethylene glycol bath [13]. The results can be attributed on a basis of the decrease in the crystallite size of ferrite films prepared through electrodeposition from the aqueous medium (39.0 nm) than that formed using electrodeposition from non aqueous medium (62.4 nm) or ferrite powders obtained using a coprecipitation technique (81.6 nm).

3.5. Kinetics of Electrodeposition Reaction. XRD patterns of Ni-Zn ferrites thin films annealed at 850°C for various periods from 1 to 4 h are shown in Figure 8. The intensity of the peaks increases with increase of annealing time. This indicates that the crystallinity of the products is improved with the annealing time.

From XRD patterns in Figure 8 the integral intensity of the (311) peak I_x of the spinel Ni-Zn ferrite phase is calculated by measuring the area under the curve [13].

The intensity of the (311) peak I_A of the film obtained after annealing for 4 h is used as a standard of crystallization, because of no increase in the intensity of the peak after 4 h. I_x has intensity of (311) peak at time t, and the fraction of crystallization in the reactive system can be calculated by the formula of $x = I_x/I_A$. Isothermal crystallization can be described by the Avrami transformation kinetic equation [13]

$$x = 1 - \exp(-kt^n), \tag{5}$$

where n is Avrami exponent (constant), depending on the details of the nucleation and growth mechanisms, x is the fraction of crystallization, k is reaction rate constant, and t is reaction time. For isothermal condition,

$$\ln[-\ln(1-x)] = \ln k + n \ln t. \tag{6}$$

Plotting of $\ln[-\ln(1-x)]$ as a function of $\ln t$ yields the values of n as shown in Figure 9. The straight line obtained showed the mechanism of the crystallization is a random nucleation, and with nucleation as the rate-determining step, could be applied. For this system, the rate of crystallization

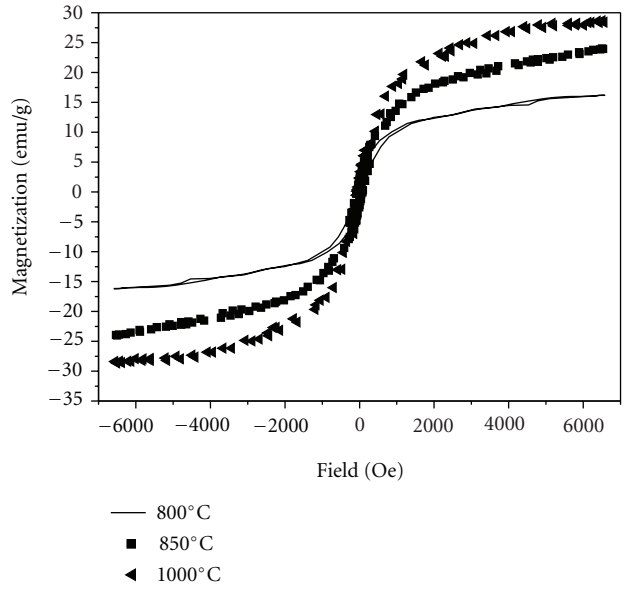

Figure 7: Effect of annealing temperature on M-H hysteresis loops of $Ni_{0.5}Zn_{0.5}Fe_2O_4$ films. Annealing temperatures: (a) 800°C, (b) 850°C, and (c) 1000°C.

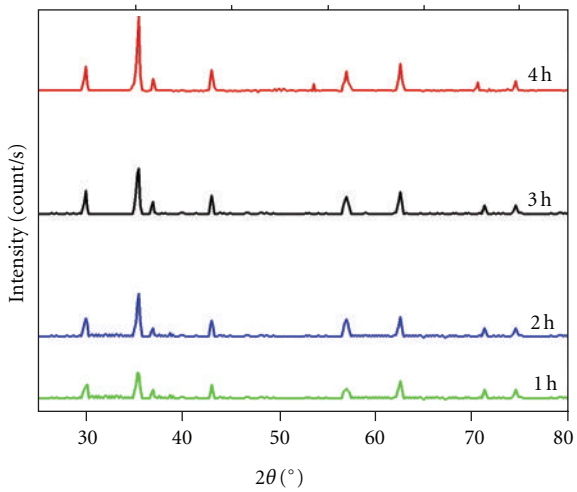

Figure 8: XRD patterns of the produced Ni-Zn ferrites annealed at 850°C for the various periods from 1 to 4 h.

is controlled by the nucleation in an assemblage of identical reactant fragments and the first-order expression is obeyed in random nucleation, as follows [13]. The temperature dependence of k could be described as a simple Arrhenius behavior, that is,

$$k = \nu \exp\left(-\frac{E}{RT}\right), \tag{7}$$

where ν is the frequency factor, E is the apparent activation energy of crystallization, and R is the gas constant. Taking logarithms of (7)

$$\ln k = \ln \nu - \left(\frac{E}{RT}\right) \tag{8}$$

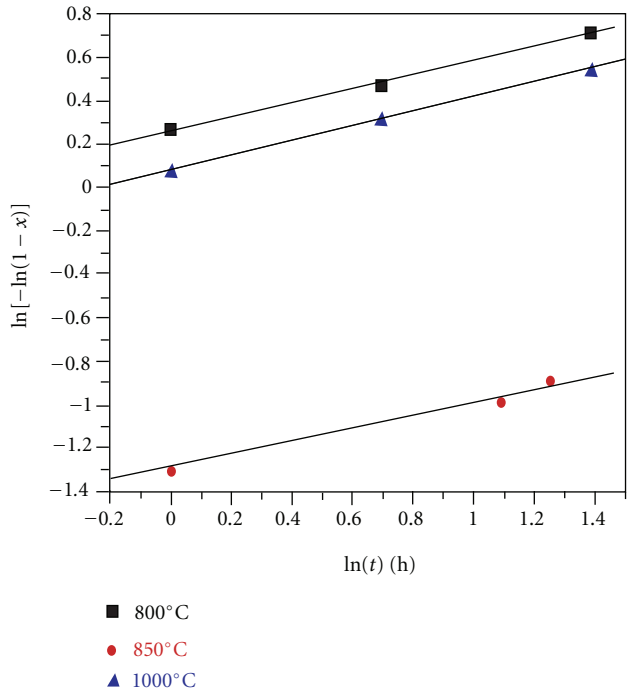

Figure 9: Avrami plot of $\ln[-\ln(1-x)]$ versus $\ln t$ for isothermal crystallization of $Ni_{0.5}Zn_{0.5}Fe_2O_4$ films annealed at different temperatures from 800 to 1000°C for different annealed times from 1 to 4 h.

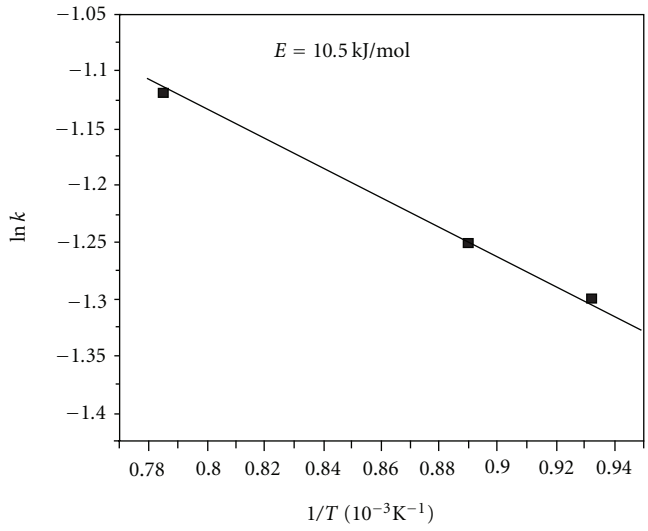

Figure 10: Arrhenius plots of $\ln k$ values against the reciprocal of the temperature for determination the activation energy of $Ni_{0.5}Zn_{0.5}Fe_2O_4$ films formed by electrodeposition technique.

By plotting the $\ln k$ values versus the reciprocal of absolute temperature Arrhenius plot was obtained. From the slope of Figure 10, the activation energy of crystallization was found to be 10.5 kJ/mole which is lower than the values of activation energies reported by Wang and Kang who used the hydrothermal process for synthesis of Ni-Zn ferrites nanoparticles [25] and that obtained by electrochemical

deposition process from ethylene glycol [13]. This can be explained by the high dielectric constant of ethylene glycol which was used as solvent in the electrochemical process; however the electrodeposition reaction required much energy to proceed.

4. Conclusions

The results can be summarized as follows.

(i) The deposition potential of (Ni-Zn)Fe_2 alloy was −0.58 V. For instance, the current density with high current efficiency 72.8% for the electrodeposition of the (Ni-Zn)Fe_2 alloy was 102mA cm^{-2}. The mechanism of nucleation and growth of electrodeposited (Ni-Zn)Fe_2 alloy was instantaneous mechanism.

(ii) $Ni_{0.5}Zn_{0.5}Fe_2O_4$ was formed after anodization in 1 M KOH and annealed at 850–1000°C for 4 h.

(iii) High saturation magnetization M_s = 28.2 emu/g was achieved for $Ni_{0.5}Zn_{0.5}Fe_2O_4$ phase annealed at 1000°C for 4 h.

(iv) The crystallization of Ni-Zn ferrite films is approached to be first-order reaction and the activation energy was found to be 10.5 kJ/mol.

References

[1] X. Shan, R. Gang, Z. Feng et al., "Preparation, microstructure and magnetic properties of Ni-Zn ferrite thin films by spin spray plating," *Journal of Wuhan University of Technology*, vol. 23, no. 5, pp. 708–711, 2008.

[2] L. Wang and F. S. Li, "Mössbauer study of nanocrystalline Ni-Zn ferrite," *Journal of Magnetism and Magnetic Materials*, vol. 223, no. 3, pp. 233–237, 2001.

[3] A. M. El-Sayed, "Effect of chromium substitutions on some properties of Ni-Zn ferrites," *Ceramics International*, vol. 28, no. 6, pp. 651–655, 2002.

[4] J. L. Gunjakar, A. M. More, K. V. Gurav, and C. D. Lokhande, "Chemical synthesis of spinel nickel ferrite ($NiFe_2O_4$) nanosheets," *Applied Surface Science*, vol. 254, no. 18, pp. 5844–5848, 2008.

[5] M. P. Horvath, "Microwave applications of soft ferrites," *Journal of Magnetism and Magnetic Materials*, vol. 215, pp. 171–183, 2000.

[6] P. A. Lane, P. J. Wright, M. J. Crosbie et al., "Liquid injection metal organic chemical vapour deposition of nickel zinc ferrite thin films," *Journal of Crystal Growth*, vol. 192, no. 3-4, pp. 423–429, 1998.

[7] S. D. Sartale, C. D. Lokhande, M. Giersig, and V. Ganesan, "Novel electrochemical process for the deposition of nanocrystalline $NiFe_2O_4$ thin films," *Journal of Physics Condensed Matter*, vol. 16, no. 6, pp. 773–784, 2004.

[8] W. Tao, S. B. Desu, and T. K. Li, "Direct liquid injection MOCVD of high quality PLZT films," *Materials Letters*, vol. 23, no. 4–6, pp. 177–180, 1995.

[9] M. Sedla, V. M. Jeca, T. Grygarb et al., "Sol-gel processing and magnetic properties of nickel zinc ferrite thick films," *Ceramics International*, vol. 26, no. 5, pp. 507–512, 2000.

[10] S. M. Chavana, M. K. Babrekarc, S. S. Moreb, and K. M. Jadhav, "Structural and optical properties of nanocrystalline Ni-Zn ferrite thin films," *Journal of Alloys and Compounds*, vol. 507, no. 1, pp. 21–25, 2010.

[11] D. Ravinder, K. Vijay Kumar, and A. V. Ramana Reddy, "Preparation and magnetic properties of Ni-Zn ferrite thin films," *Materials Letters*, vol. 57, no. 26-27, pp. 4162–4164, 2003.

[12] S. D. Sartale, G. D. Bagde, C. D. Lokhande, and M. Giersig, "Room temperature synthesis of nanocrystalline ferrite (MFe_2O_4, M = Cu, Co and Ni) thin films using novel electrochemical route," *Applied Surface Science*, vol. 182, no. 3-4, pp. 366–371, 2001.

[13] A. E. Saba, E. M. Elsayed, M. M. Moharam, M. M. Rashad, and R. M. Abou-Shahba, "Structure and magnetic properties of Ni x Zn_{1-x} Fe_2O_4 thin films prepared through electrodeposition method," *Journal of Materials Science*, vol. 46, no. 10, pp. 3574–3582, 2011.

[14] Y. N. Nuli and Q. Z. Qin, "Nanocrystalline transition metal ferrite thin films prepared by an electrochemical route for Li-ion batteries," *Journal of Power Sources*, vol. 142, no. 1-2, pp. 292–297, 2005.

[15] I. Zhitomirsky, A. Petric, and M. Niewczas, "Nanostructured ceramic and hybrid materials via electrodeposition," *Journal of the Minerals Metals & Materials Society*, vol. 54, no. 9, pp. 31–34, 2002.

[16] S. Bijani, M. Gabs, L. Martínez, J. R. Ramos-Barrado, J. Morales, and L. Sánchez, "Nanostructured Cu2O thin film electrodes prepared by electrodeposition for rechargeable lithium batteries," *Thin Solid Films*, vol. 515, no. 13, pp. 5505–5511, 2007.

[17] C. H. Wang, K. W. Cheng, and C. J. Tseng, "Photoelectrochemical properties of AgInS2 thin films prepared using electrodeposition," *Solar Energy Materials and Solar Cells*, vol. 95, no. 2, pp. 453–461, 2011.

[18] J. C. Ballesteros, P. Díaz-Arista, Y. Meas, R. Ortega, and G. Trejo, "Zinc electrodeposition in the presence of polyethylene glycol 20000," *Electrochimica Acta*, vol. 52, no. 11, pp. 3686–3696, 2007.

[19] S. O. Pagotto, C. M. De Alvarenga Freire, and M. Ballester, "Zn-Ni alloy deposits obtained by continuous and pulsed electrodeposition processes," *Surface and Coatings Technology*, vol. 122, no. 1, pp. 10–13, 1999.

[20] K. M. Yin and B. T. Lin, "Effects of boric acid on the electrodeposition of iron, nickel and iron-nickel," *Surface and Coatings Technology*, vol. 78, no. 1–3, pp. 205–210, 1996.

[21] A. I. Inamdar, S. H. Mujawar, S. B. Sadale et al., "Electrodeposited zinc oxide thin films: nucleation and growth mechanism," *Solar Energy Materials and Solar Cells*, vol. 91, no. 10, pp. 864–870, 2007.

[22] S. D. Sartale, C. D. Lokhande, and M. Muller, "Electrochemical synthesis of nanocrystalline CuFe2O4 thin films from non-aqueous (ethylene glycol) medium," *Materials Chemistry and Physics*, vol. 80, no. 1, pp. 120–128, 2003.

[23] C. D. Lokhande, S. S. Kulkarni, R. S. Mane, and S. H. Han, "Copper ferrite thin films: single-step non-aqueous growth and properties," *Journal of Crystal Growth*, vol. 303, no. 2, pp. 387–390, 2007.

[24] M. M. Rashad, E. M. Elsayed, M. M. Moharam, R. M. Abou-Shahba, and A. E. Saba, "Structure and magnetic properties of $Ni_xZn_{1-x}Fe_2O_4$ nanoparticles prepared through co-precipitation method," *Journal of Alloys and Compounds*, vol. 486, no. 1-2, pp. 759–767, 2009.

[25] H. W. Wang and S. C. Kung, "Crystallization of nano-sized Ni-Zn ferrite powders prepared by hydrothermal method," *Journal of Magnetism and Magnetic Materials*, vol. 270, pp. 230–236, 2004.